Journal of Physical Chemistry C
https://doi.org/10.1021/acs.jpcc.0c08981

Limiting Domain Size of MoS_2: Effects of Stoichiometry and Oxygen

Rimei Chen,[†] Andrew R. Konicek,[‡] Arben Jusufi,[‡] Chris E. Kliewer,[‡] Aditya Jaishankar,[‡] Alan Schilowitz,[‡] and Ashlie Martini[*,†]

†*Department of Mechanical Engineering, University of California Merced, Merced, California, USA*

‡*Corporate Strategic Research, ExxonMobil Research and Engineering Company, Annandale, New Jersey, USA*

E-mail: amartini@ucmerced.edu

Abstract

Reactive molecular dynamics simulations of MoS_2 crystallization from amorphous precursor materials showed that crystal domain size decreased due to excess S or O, relative to the stoichiometric case. Simulation results were corroborated by comparison of calculated limiting domain sizes to experimental measurements of MoS_2 crystals grown from thermal decomposition of molybdenum dithiocarbamate. Then, the simulations were used to evaluate two previously proposed domain growth mechanisms – thermodynamic and kinetic; both were shown to contribute to MoS_2 domain growth and, importantly, to stopping growth at a limiting size. It was shown that S-rich or O-containing precursor materials can inhibit grain growth (i) thermodynamically, by increasing the amount of S at domain edges which decreases boundary energy, making them more stable and lowering the driving force for growth, and (ii) kinetically, by decreasing the probability of Mo-S interactions at domain edges that would otherwise contribute to domain growth. The simulations explain how each of these mechanisms deter-

mines the effect of precursor composition on MoS_2 domain size and, further, suggest avenues for tunable MoS_2 synthesis to achieve application-specific domain size.

Introduction

Molybdenum disulfide (MoS_2) possesses outstanding catalytic,[1–3] electronic,[4–7] and tribological[8] properties. However, the performance of MoS_2-based applications strongly depends on the lateral dimensions of the crystalline grains, also referred to as the domain size. For example, scanning tunneling microscopy showed that the morphology and electronic structure of MoS_2 clusters is dependent on domain size which suggested domain size also affected catalytic activity.[9] Size-dependent optical properties of MoS_2 nanoparticles were observed in a study that found average emission lifetime increases with increasing particle size.[10] Also, the exchange current density of MoS_2 nanoparticles has been found to be higher for particles with longer edges.[11] Further, from a tribological perspective, larger domain sizes provide fewer edge sites that can oxidize in air and inhibit sliding.[12,13]

The size of MoS_2 domains are determined by the material synthesis process and conditions. Various methods are available for MoS_2 synthesis, including chemical vapor deposition (CVD)[14–19] and solution chemical processing.[18–20] CVD produces MoS_2 films on a substrate by sulfurization of elemental Mo[16] or Mo-based compounds.[21–25] This method forms gaseous MoS_2 that is deposited on a substrate, resulting in large-area and highly uniform MoS_2 films. The size of the MoS_2 domains produced by CVD typically ranges from a few nanometers[26] to a few micrometers.[21–25] Alternatively, solution chemical processing produces MoS_2 films from thermal decomposition of $(NH_4)_2MoS_4$ followed by annealing.[27] The size of MoS_2 domains produced from this method is smaller than that from the CVD method and is typically in the range of a few nanometers.[28,29] MoS_2 can also form in tribological applications from thermally and shear-driven decomposition of lubricant additives such as molybdenum dithiocarbamate (MoDTC).[30] MoS_2 formed through decomposition of lubricant additives plays a critically important role in enabling the energy effi-

cient operation of moving mechanical components. In any of these synthesis methods, domain size is affected by the composition of the precursor elements as well as the substrate composition and morphology.[31–35] Here, we focus on the thermal decomposition method of MoS_2 formation that is relevant to lubricated mechanical systems.

Synthesis conditions affect domain size because they determine the density of nucleation and kinetic growth rate of crystalline regions within the material. The growth mechanisms of various materials have been investigated theoretically[33,36–38] and experimentally.[31,38–40] Crystal growth is predicted to follow a power-law function for highly pure, single-phase systems.[41] However, due to impurities that are unavoidable during synthesis, crystal growth will slow and then stop at some finite maximum domain size; this maximum is called the limiting domain size.[36,42,43] Two mechanisms have been proposed to describe how impurities inhibit crystal growth. The first is by eliminating the force driving growth at domain boundaries (thermodynamic mechanism). This decrease of driving force may be caused by solute atoms that migrate on the domain boundaries which decreases the excess free energy of the boundary.[38,43,44] The second is by decreasing the mobility of the boundaries of the crystalline domains (kinetic mechanism). In this mechanisms, studies have shown that crystal growth is slowed by a retarding force from solute drag.[36,39,42,45] Solute drag is attributed to interactions between the domain boundaries and solute atoms, so drag increases with the accumulation of impurities at the edges of a domain.

Previous studies have reported that MoS_2 domain growth can be driven thermodynamically[46] or kinetically.[33,47] Both proposed mechanisms predict that more impurities will lead to smaller domains. This is consistent with observations from MoS_2 synthesis that varying the ratio of Mo and S in precursor materials leads to different domain size.[33,34] However, these theories have not been applied to understand how and why MoS_2 domain growth stops at a limiting domain size. Further, the exact relationship between precursor composition and limiting domain size is not known because the underlying mechanisms are based on atomic-scale features at the boundaries of individual domains. Unfortunately, these features cannot easily be measured using experimental tools during synthesis. An alternative is atomistic simulations that provide an *in situ* view of the struc-

ture and chemistry of domain edges during the growth process with precisely controlled precursor compositions. While density functional theory (DFT) has been used to model MoS_2 growth,[48–50] the size scale of first principles calculations limits their ability to model physically representative domain sizes.Instead, reactive molecular dynamics (MD) simulations that use a bond-order approach to capture the formation and breaking of chemical bonds can be applied.[51,52] Parameters within the ReaxFF formalism have recently been developed for MoS_2 [53] as well as MoS_2 in the presence of oxygen.[54] Simulations using a modified form of this potential have shown that oxygen inhibits grain growth,[55] but they have not been applied to study limiting domain size.

Given the size-dependence of MoS_2 material properties and the effect of those properties on the performance of MoS_2-based applications, it is desirable to precisely control the size of MoS_2 domains during synthesis. However, the effects of synthesis conditions on the fundamental mechanisms underlying domain growth and limiting domain size are not fully understood. To address this, we use reactive MD simulations to study the relationship between precursor composition – specifically, the relative amounts of Mo, S and O – and limiting domain size. Domain sizes predicted by the simulation are corroborated by comparison to experimental measurements of MoS_2 crystals produced by thermal decomposition of MoDTC. The simulations then provide atomic-scale information about the domains that enable testing of existing theories for domain growth. The results contribute to the fundamental understanding needed to ultimately tune the domain size of MoS_2 to achieve optimized material properties for application-specific performance, particularly for lubricated systems in which additives with varying Mo:S:O ratios form MoS_2 films that increase energy efficiency and component life.

Methods

Simulations

The model system consisted of an amorphous layer of Mo, S and O atoms sandwiched between two crystalline MoS_2 layers as shown in Fig. 1a. Nine models were created where the amorphous layer

comprised different ratios of Mo, S and O. The Mo:S ratios modeled were 1:2, 1:3, and 1:5, and the percent oxygen was 0, 10 or 20%, as shown in Fig. 1b. All model systems had the same total number of atoms. Periodic boundaries were applied in the x- and y-directions and a fixed boundary was applied in the z-direction; the position of the bottom MoS_2 layer was fixed in all directions. Molecular dynamics simulations were carried out using the LAMMPS package[56] and OVITO[57] was used for visualization. Atomic interactions were modeled by the ReaxFF potential[53,54] for Mo/S/O with modified parameters[55] with a time step of 0.25 fs. This potential has been found to be able to capture the crystallization of MoS_2 from amorphous materials in previous studies.[55]

Crystallization of the middle layer for each model was simulated using the same procedure as reported previously.[55,58] First, amorphous material was created by heating a single layer of crystalline MoS_2 to 5300 K and then rapidly quenching to room temperature. The system was then equilibrated at room temperature, and a pressure of 50 GPa was applied in the z-direction using a Parrinello-Rahman barostat. After reaching stable potential energy, the amorphous system was inserted between two crystalline MoS_2 layers, as shown in Fig. 1a. The interactions between the crystalline MoS_2 layers and the amorphous layer were restricted to van der Waals only. The crystalline layers were rigid, and a normal force was applied at the top layer to maintain a pressure of 50 GPa. This pressure mimicked the local stress conditions that may be present at asperity-asperity contacts in highly loaded lubricated interfaces. High pressure was also used to accelerate the crystallization.

The dimensions of the simulation box at this stage were $20.6 \times 19.6 \times 3.8$ nm^3 in x-, y-, and z-directions, respectively. In a previous study, simulations with lateral dimensions of 10×10 nm^2, 20×20 nm^2 and 30×30 nm^2 confirmed that domain growth rates do not depend on box size and that the 20×20 nm^2 system is large enough to capture the maximum domain sizes.[55] Next, this sandwiched system was equilibrated for 0.2 ns at room temperature with a Nosé-Hoover thermostat. After equilibration the temperature of the system was increased from room temperature to 4000 K using a Langevin thermostat with a damping parameter of 250 fs. The simulation was then run at 4000 K for 1.5 ns, where the high temperature was used to accelerate the crystallization

process such that it could be observed within the short duration of the simulation. Note that 4000 K is above the melting temperature of MoS_2 at atmospheric pressure, but simulations performed at different pressures indicated that 4000 K was below the melting temperature at the high pressure conditions studied here.

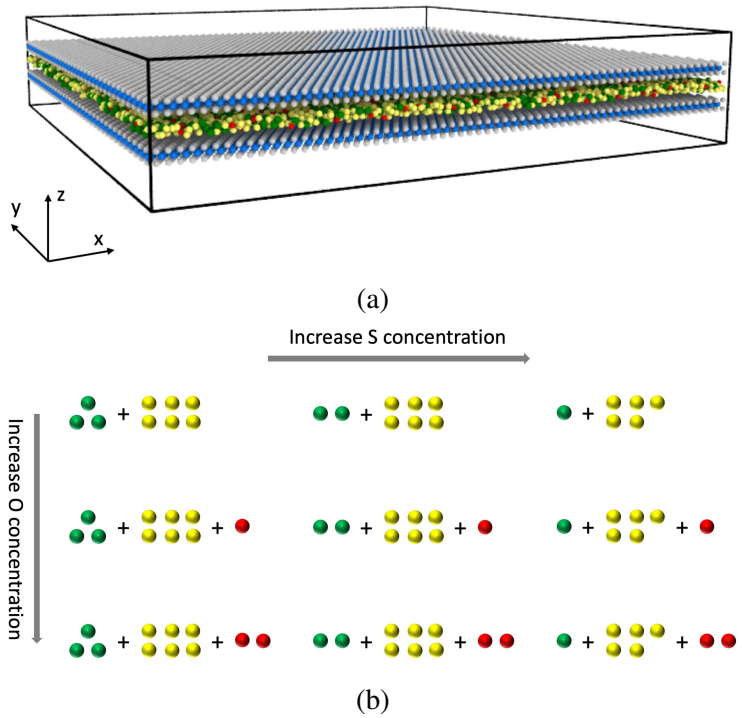

Figure 1: (a) Perspective view of the simulation model where an amorphous layer comprising Mo, S and O is between two crystalline MoS_2 sheets. (b) Schematic of the concentrations of Mo, S, and O in the amorphous layer for the nine different model systems. In both figures, the molybdenum and sulfur atoms in the amorphous material are shown as green and yellow, and are blue and grey in the crystalline confining walls, respectively. The oxygen atoms are shown in red.

During the simulation, the atomic position of each atom in the middle layer was used to determine if it was part of crystalline or amorphous material. For each molybdenum atom, first, we calculated its distance from all sulfur atoms. If the distance was within a pre-determined distance range, then the S atom was considered to be a neighbor of the Mo atom. If the number of neighbor atoms was six, we then calculated the angles between the Mo atom and its neighbor S atoms. If all angles were within the neighbor angle range, then this Mo atom was defined as a crystal atom. The same procedure was applied to the S atoms, except that the number of neighbor atoms in the

criterion was three. The neighbor distance and angle ranges used in this calculation were reported previously.[55] Using these values, the degree of crystallinity of a MoS_2 sheet was quantified as the percent of crystalline Mo atoms relative to the total number of Mo atoms in the system. After characterizing the crystallinity, the size of the crystalline domains in the middle layer was quantified. We defined a domain based on the distance between crystalline atoms. If the distance between a crystalline Mo atom and S atom was within the maximum distance used to determine crystallinity, then these atoms were said to be in the same domain. The atoms at the edge of a domain were identified using the same maximum distance criterion. The size of each domain was then calculated as twice the maximum distance from the edge atoms to the domain center.

Experiments

MoS_2 crystals were grown from thermal conversion of molybdenum dithiocarbamate on iron. First, a copper grid was covered with a 200 mesh holey carbon film. That film was used as a substrate to deposit an iron thin film on the order of tens of nanometers thick. Then, the sample was placed in an air oven and the temperature was ramped from ambient to 350 °C over a one hour time period and held at 350 °C for two hours before being cooled back to room temperature. This step burned away the holey carbon film leaving only the metal film behind. The sample was then cleaned by dipping sequentially into ethanol and heptane for 20 seconds each. Then this metal-coated copper grid was soaked in a solution of heptane with 0.85 wt% MoDTC, using a liquid level extending approximately 1 cm above the grid, and left uncapped to allow for solvent evaporation overnight. After the soak, the sample was placed in a vacuum furnace and the temperature was ramped to 350 °C at 3 °C/min. and then held at 350 °C for 1 hour, which thermally converted the MoDTC friction modifier into MoS_2 crystals.

The surface was examined in the bright field transmission electron microscope (TEM) imaging mode of a JEOL 200F TEM/STEM at an accelerating voltage of 200 kV. Images were collected using a Gatan One View CCD camera system and Gatan Digital Micrograph software. The focus was on regions of the copper grid between mesh lines where there was only the presence of the thin

metal film and any MoS_2 crystals. TEM micrographs were processed using a custom MATLAB algorithm identify the locations and orientations of the MoS_2 crystals. The process identified individual MoS_2 sheets, determined which sheets belonged to the same crystal using their centroid location and rotation angle, and then calculated the number of layers per crystal and average size of those crystals. Detailed information about the domain identification and size calculation algorithm is available in the Supporting Information.

Results

Domains were identified and their size was tracked as a function of time from simulations with varying stoichiometry and oxygen content. Representative domains from a simulation with a Mo:S ratio of 1:2 and 0% oxygen at simulation run times of 0.02 ns and 0.04 ns are shown in Figs. 2a and 2b, with the corresponding distribution of domain sizes in Fig. 2c. The average of the three largest sizes was calculated to represent the domain size at each time step. For the examples in Fig. 2c, the three largest domains are shown in blue in the histogram and the average domain size is identified by a dashed line. In these cases, the average domain size was 2.9 nm at 0.02 ns and 8.2 nm at 0.04 ns. The average domain size calculation was repeated for all time steps in each simulation.

The average domain size as a function of simulation time for different precursor material compositions is shown in Fig. 3. In all cases, the domain size increases and then saturates at a stable value, i.e. the limiting domain size. Also, larger limiting domain sizes correspond to longer time required for the domains to saturate at their limiting value. Comparing the different model cases, the simulation with a Mo:S ratio of 1:2 and no oxygen has the longest saturation time and the largest limiting domain size, while the shortest saturation times and limiting domain sizes are observed for the Mo:S ratios of 1:3 and 1:5 with 20% oxygen.

In the simulations, the limiting domain size was calculated by averaging the domain size over the last 0.5 ns of the 1.5 ns simulations. A contour plot of the limiting domain size at different

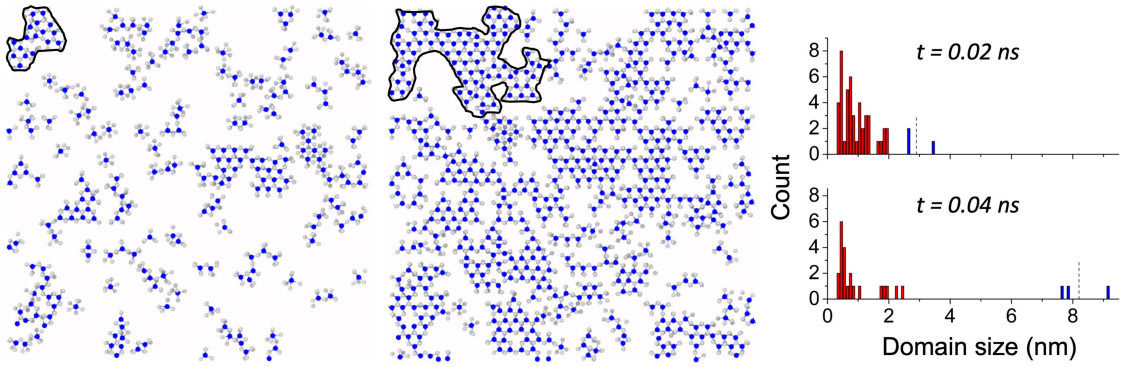

(a) (b) (c)

Figure 2: Top view snapshots of the crystalline atoms, with the perimeter of one representative domain traced from a model with a Mo:S ratio of 1:2 and 0% oxygen at (a) 0.02 ns and (b) 0.04 ns with (c) the corresponding domain size distributions. The largest three domains are shown in blue and the average of the three largest domain sizes are represented as dashed lines in the distribution plots.

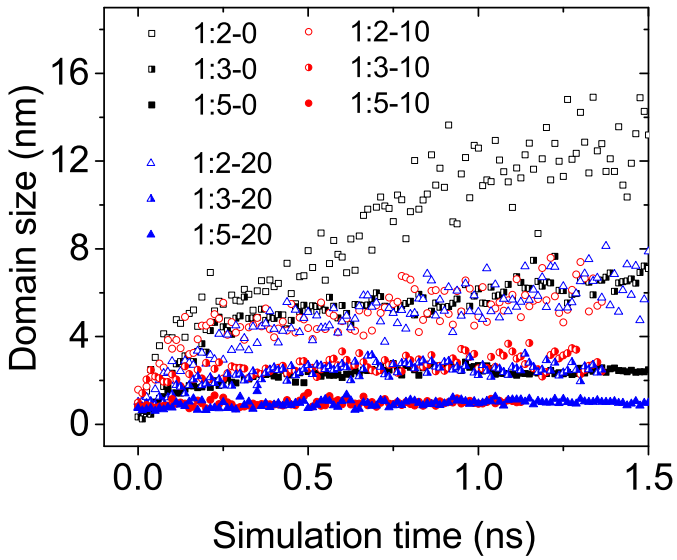

Figure 3: The average size of the three largest MoS_2 domains increases with simulation time under different simulation conditions. Symbol shape reflects the oxygen content – squares 0%, circles 10% and triangles 20% – and symbol fill reflects the Mo:S ratio of the precursor amorphous material – hollow 1:2, half-solid 1:3 and solid 1:5.

simulation conditions is shown at Fig. 4, where red represents larger domains and blue corresponds to smaller domains. It can be observed that domain size decreases with increasing sulfur and oxygen content. This is consistent with findings from prior studies where the Mo:S ratio of CVD precursor materials was shown to affect the size of synthesized MoS_2 domains and ratios closer to 1:2 resulted in the largest domains.[33,34] Note that a previous experimental study reported that oxygen can facilitate the growth of larger domains, and the observation was attributed to etching of domain boundaries that decreased the nucleation density.[59] This is not observed in our simulations where domain growth is much faster than the rate of domain etching due to the finite supply of oxygen.

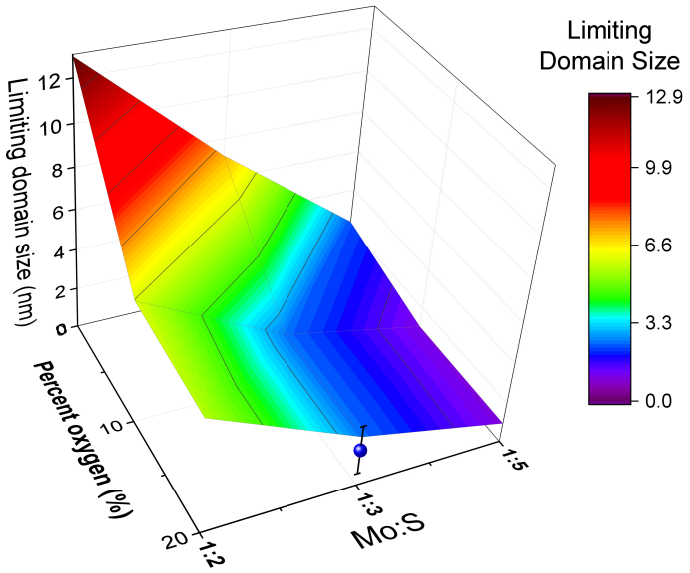

Figure 4: The limiting domain size at different simulation conditions where domain size decreases from red to blue. The experimental data for MoDTC (corresponding to Mo:S ratio of 1:3 and 20% oxygen) is shown as a symbol with color representing the measured average domain size of 1.8±1.2 nm.

The limiting domain sizes determined from the simulations were next analyzed in the context of the complementary experiments. A TEM image of MoS_2 crystals grown from thermal conversion of MoDTC on an Fe thin film is shown in Fig. 5a, with individual crystals highlighted using false coloring in Fig. 5b. The domain size distribution for this sample is shown in Fig. 5c. The average domain size was calculated to be 1.8 ±1.2 nm. These MoS_2 crystals were grown from

MoDTC, which corresponds to simulations of precursor material with a Mo:S ratio of 1:3 and oxygen concentration of 20%. The limiting domain size for that simulation case was 2.5 $\pm$ 0.2 nm, which agrees well with the average experimental grain size for MoS_2 grown from MoDTC of 1.8 $\pm$1.2 nm, as shown by the symbol in Fig. 4. Note that the largest domains in the simulations can be compared to the average domain size identified in experiments because only the largest domains from multiple layers are detected by the algorithm used for image analysis in the experiments (as opposed to the single layer in simulations). This quantitative consistency and the general agreement with expected trends for domain growth suggest that the simulations are capturing a physically realistic domain growth process.

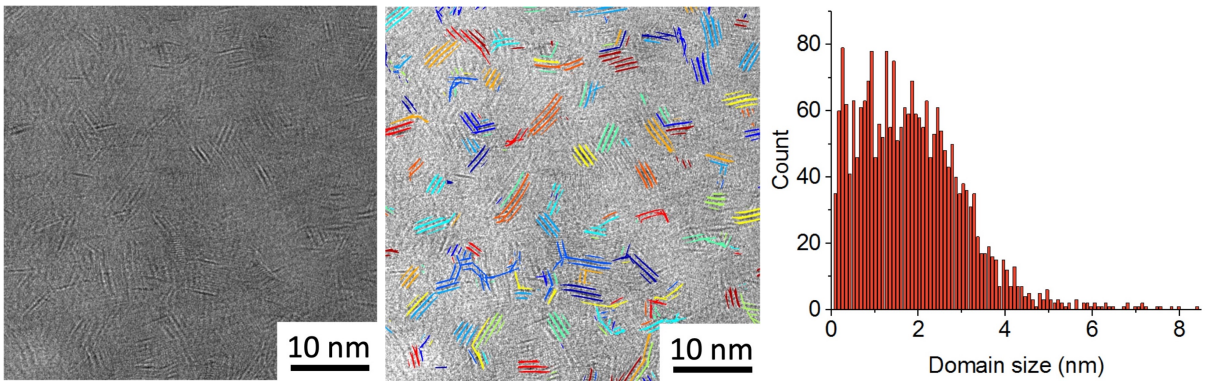

(a) (b) (c)

Figure 5: (a) TEM image of an iron film covered with MoS_2 crystals. (b) The same region as in (a) where the MoS_2 sheets are false colored with arbitrary, contrasting colors. Sheets identified as being in the same crystal are colored the same. (c) Size distribution of the MoS_2 crystals.

Discussion

Crystallization of MoS_2 occurs through nucleation and domain growth. The rate of nucleation is expected to exhibit an Arrhenius dependence and is therefore a function of the nucleation energy barrier and the temperature.[58] As expected, given the high temperature conditions of the simulations here, nucleation occurred rapidly at the start of the simulation for all cases. Therefore, it can be assumed that the limiting domain size was determined by the domain growth process. Prior research has suggested that domain growth can be decelerated by two mechanisms: (i) kinetic, where

solute drag lowers the mobility of the domain boundary;[36,37] and (ii) thermodynamic, through decreased driving force at the domain boundary (i.e. boundary energy).[43] Both of these mechanisms predict that the presence of reactive impurities will inhibit grain growth and therefore decrease limiting domain size. In the case of MoS_2, the impurities are excess sulfur (Mo:S ratios other than 1:2) and the presence of oxygen. Therefore, these mechanisms predict behavior consistent with the simulation observations (Fig. 4) that limiting domain size decreases with increasing S or O in the amorphous precursor material.

For both mechanisms, domains grow through adsorption (also called attachment or deposition) of atoms at domain boundaries. For domain growth driven by thermodynamics, the incoming atoms diffuse along the boundary to reach sites with the lowest free energy. However, if the diffusion is not fast enough, adatoms may occupy and be trapped in less energetically favorable sites, leading to a kinetic domain growth process. The relative rates of atom adsorption and diffusion determine if the domain growth process is driven thermodynamically (diffusion dominant), kinetically (adsorption dominant), or both.[60] Prior studies of MoS_2 formation have reported similar adsorption ($\sim 2.0\ eV$) and diffusion ($\sim 1.84\ eV$) energy barriers.[47] Since diffusion/adsorption rates are direct functions of these energy barriers, it is likely that both thermodynamics and kinetics contribute to domain growth for MoS_2.

Thermodynamically controlled domain growth is an energy reduction process to reach the minimum Gibbs free energy of the system. In this context, domain size no longer increases when the system reaches an equilibrium state, i.e. its minimum energy. To quantify the contribution of this mechanism, the boundary energy for each case was determined from the simulations. Boundary energy γ was calculated from the difference between the total potential energy of the atoms in a given domain (E_d) and the energy of those atoms in an ideal MoS_2 lattice as:[61]

$$\gamma = \frac{E_d - N_{Mo,d} \times E_{Mo} - N_{S,d} \times E_S}{L} \tag{1}$$

where $N_{Mo,d}$ and $N_{S,d}$ are the number of Mo atoms and S in a given domain, E_{Mo} and E_S are the

potential energies of Mo and S in crystalline MoS_2, and L is the perimeter of the domain. The potential energies were calculated to be E_S = -90.9 Kcal/mole and E_{Mo} = -270.2 Kcal/mole using per-atom energies from simulations of a perfectly crystalline monolayer of MoS_2 subject to the pressure and temperature conditions used in this study. The boundary energy was then calculated for the largest three domains after the domain size reached steady state for each simulation condition. As shown in Fig. 6a, the boundary energy increases with limiting domain size, where smaller domains and smaller boundary energy is observed in cases with more impurities. This is consistent with prior studies that have shown that impurities at the boundaries of a domain increase its thermal stability by decreasing the boundary energy.[38,43,44] So, thermodynamic equilibrium can be attained much faster in the presence of impurities, resulting in less diffusion and smaller domains.

The next question is how impurities decrease the grain boundary energy. If there are no impurities, the concentration of S atoms at the edges of crystalline domains should be 66.7%. However, in sulfur-rich conditions, there is an energetic preference for the growth of S-terminated domain edges.[62] Additionally, the presence of oxygen causes the formation of Mo oxysulfide and MoO_3,[55,59] which will result in a sulfur-rich condition, leading to growth of S-terminated domain edges. DFT calculations of MoS_2 formation showed that S-termination is energetically preferred (compared to Mo-termination),[48] so more S-termination should correspond to lower boundary energy. This was quantified in the simulations as the amount of excess S (N_{ex} relative to the ideal stoichiometry) as calculated by:

$$N_{ex} = \frac{N_{S,d} - 2N_{Mo,d}}{N_{tot,d}} \tag{2}$$

where $N_{tot,d}$ is the total number of atoms in given domain. This formulation captures the expectation that more S-termination will increase the amount of excess sulfur but, for a given-S termination, the excess S will be smaller for larger domains. The calculation was performed for the largest three domains during steady-state at each simulation condition. As shown in Fig. 6b, the boundary energy decreases with increasing excess S. The variation in boundary energy for the different cases reflects the fact that the stoichiometry of the domain edges differs depending on the initial composition of the amorphous material. Specifically, this analysis shows that impurities increase

the S-termination of domain boundaries which then reduces the boundary energy and enhances the thermal stability of domains, leading to smaller and more stable limiting domain size.

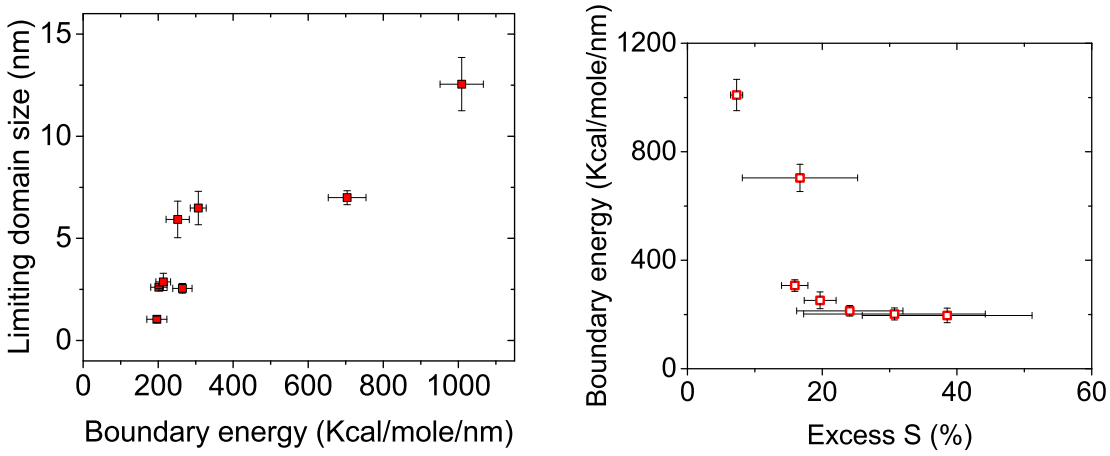

(a) (b)

Figure 6: (a) Domain boundary energy increases with limiting domain size and (b) boundary energy decreases with increasing excess S which results from the presence of more impurities.

Impurities in the system can also inhibit grain growth through the kinetic mechanism by increasing drag from the solute,[45] in this case, from the amorphous material. To evaluate the effect of solute drag on domain growth, a constant drag was assumed during the growth process.[42] This assumption, as opposed to a size-dependent drag,[36] was reasonable for our model system because the concentration of S atoms in the solute did not increase significantly during domain growth. First, the domain mobility was calculated by fitting to the domain size vs. time data in Fig. 3. Then, drag was calculated as the domain mobility divided by the limiting domain size;[36] details for this calculation and the mobility parameter are given in the Supporting Information. The relationship between the limiting domain size and calculated drag is shown at Fig. 7a. As expected based on the kinetic domain growth mechanism,[36,39] the limiting domain size decreases with increasing drag, which indicates that larger drag slows domain growth, leading to a smaller limiting domain size.

Drag is associated with interactions at the interface between crystalline domains and the surrounding solute that prevent atom adsorption leading to domain growth.[37] Atom adsorption was

quantified in the simulations in terms of the probability of adsorption of either S or Mo atoms at the edges of domains. First, the probability of domain growth through adsorption of S at the domain edge P_S was calculated as the product of the fraction of Mo edge sites and S atoms in the amorphous material:

$$P_S = \left(\frac{2N_{Mo,e}}{2N_{Mo,e}+N_{S,e}+N_{O,e}}\right) \times \left(\frac{N_{S,a}}{N_{tot,a}}\right) \tag{3}$$

where N_e is the number of atoms at the edges of domains and N_a is the number of atom in the amorphous material. The total number of atoms at the edge is calculated as $N_{tot,e} = 2N_{Mo,e} + N_{S,e} + N_{O,e}$, where the factor 2 represents the two available sites from a Mo edge atom; implied is a factor of 1 for the S edge atoms. Similarly, the probability of growth through adsorption of Mo atoms P_{Mo} was calculated as:

$$P_{Mo} = \left(\frac{N_{S,e}}{2N_{Mo,e}+N_{S,e}+N_{O,e}}\right) \times \left(\frac{N_{Mo,a}}{N_{tot,a}}\right) \tag{4}$$

However, for cases with oxygen, the number of available Mo atoms in the amorphous material $N_{Mo,a}$ excluded atoms bonded to O atoms. This criterion was based on the observation that the formation of Mo oxides or oxysulfide is more energetically favorable than the decomposition of those species.[63]

There is an energy barrier for bonding to occur at each possible reaction site, so only a fraction of the total number of available sites might result in adsorption. However, at the high temperature conditions studied here, it is assumed that the thermal energy is greater than potential barrier such that the adsorption rate is directly proportional to the total probability of adsorption, $P_{tot} = P_S + P_{Mo}$. To compare this probability from case to case, the detrimental effect of drag was quantified as $P_{drag} = 1 - P_{tot}/0.5$, where 0.5 is the probability for the ideal case where the Mo:S ratio at the edge and in the amorphous material are both 1:2. The relationship between the drag and the probability of drag-induced interactions (P_{drag}) is shown in Fig. 7b. The drag increases with increasing probability of growth-inhibiting atomic interactions. Impurities, specifically S or O, increase this probability and therefore increase drag, which leads to a smaller limiting domain

size.

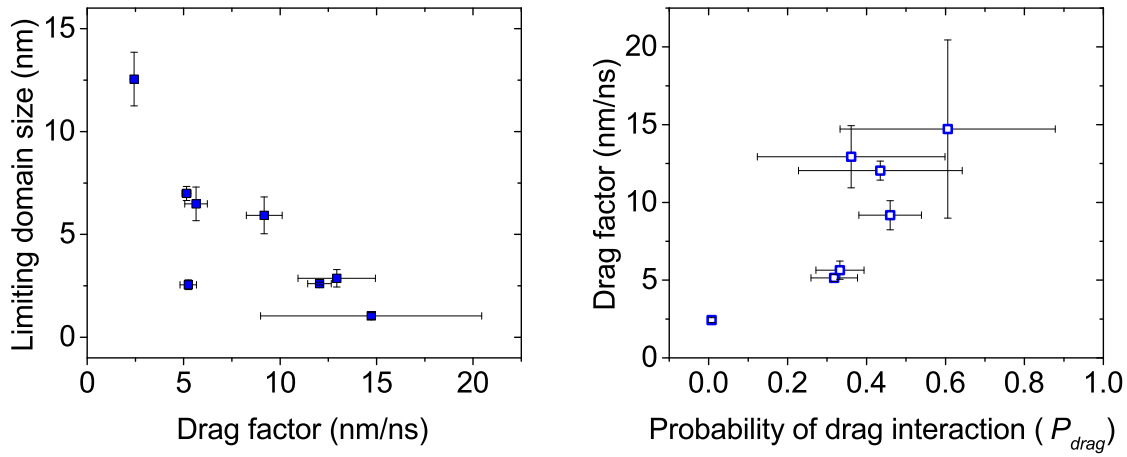

(a) (b)

Figure 7: (a) The limiting domain size decreases as drag at the domain boundary increases. (b) Drag is caused by interactions between atoms at the edges of crystalline domains and atoms in the amorphous solute, so drag increases with the probability of these interactions.

From the above analyses, it is evident that excess S and the presence of O atoms can decrease domain size via both thermodynamic and kinetic mechanisms. Excess S increases the energetic stability of the domains, which slows their growth thermodynamically; excess S also increases the drag from the solute by decreasing the probability of Mo-S interactions, which slows domain growth kinetically. The effect of oxygen on domain size is more complex. First, oxygen can inhibit the kinetic mechanism directly by impeding Mo-S interactions at domain edges. Second, the presence of O atoms in the amorphous material leads to the formation of Mo oxides and oxysulfide that result in excess S, which affects the thermodynamic mechanism as explained above.

Using the data from the simulation, we can evaluate if the dominant effect of oxygen is to increase the concentration of sulfur (thermodynamics) or impede Mo-S interactions (kinetics). For the simulation with a nominal Mo:S ratio of 1:2 and 20% oxygen, the effective Mo:S ratio at steady-state is 1:2.6 (after excluding the Mo oxide and oxysulfide species). Simple linear interpolation with the domain sizes of the no-oxygen 1:2 and 1:3 cases predicts that the limiting domain size at a Mo:S ratio of 1:2.6 would be 8.2$\pm$0.6 nm. In the simulation, the 1:2 with 20% oxygen case had a limiting domain size of 6.5$\pm$0.8 nm, smaller than the prediction that assumes only the

thermodynamic mechanism. A similar analysis was performed for the other oxygen-containing cases which showed larger predicted domain size than observed in simulations, as reported in Table S2. The linear fit used here is a rough approximation, but the difference between predicted and actual domain sizes is statistically significant. This difference may be attributable to the direct role of oxygen to impede Mo-S interactions through the kinetic mechanism. Therefore, this analysis suggests that oxygen affects limiting domain size both thermodynamically (increasing the excess sulfur concentration in the solute) and kinetically (impeding Mo:S interactions at domain edges).

Conclusions

Reactive molecular dynamics simulations were used to capture MoS_2 domain growth from an amorphous precursor comprising controlled amounts of Mo, S and O atoms. The limiting domain size decreased with the increasing S or O, relative to the ideal 1:2 with 0% oxygen case, consistent with behavior expected for growth of crystalline domains in the presence of impurities. Further, the limiting domain size predicted by the simulation for the 1:3 and 20% oxygen case was consistent with experimental measurements of domain size for MoS_2 grown from thermal decomposition of MoDTC.

Two previously proposed domain growth mechanisms – thermodynamic and kinetic – were evaluated using the simulations reported in this manuscript. For both mechanisms, we first tested whether or not the mechanism was contributing to MoS_2 domain growth and, importantly, the stopping of growth at a limiting size. Then, we explored how a S-rich composition or presence of O in the precursor material could inhibit grain growth through these two mechanisms. For the thermodynamic mechanism, we demonstrated that the limiting domain size increased with grain boundary energy, confirming the contribution from thermodynamics. Then, it was shown that the presence of S and O impurities could decrease boundary energy by increasing the amount of excess S at domain edges, thereby inhibiting growth. Next, the kinetic mechanism was tested by calculating the drag factor associated with drag from the solute acting to slow domain growth. An inverse

relationship between limiting domain size and drag factor was observed, suggesting that the kinetic mechanism contributes to MoS_2 domain growth as well. The origin of this mechanism was shown to be the probability of atomic interactions at domain boundaries leading to growth. These analyses confirm that both the thermodynamic and kinetic mechanisms are likely to contribute to MoS_2 domain growth and determine the precursor-dependent size of those domains. Neither mechanism was found to be dominant in the simulations studied here, but their relative contributions likely depend on material composition and conditions, potentially suggesting avenues to magnify one mechanism or the other during the growth process.

These findings have important implications for applications where the size of MoS_2 domains determines functionality or performance. The simulations showed that the largest domain sizes can be achieved with a 1:2 stoichiometric precursor material and no oxygen or other impurities. In practice, this ideal condition may not be achievable, but the outcomes of this study emphasize the significance of the precursor composition, particularly the Mo:S ratio, on final domain size. Further, for some applications, it may be desirable to achieve specific domain sizes, as opposed to simply the largest. For such cases, the results of this study suggest avenues for tuning limiting domain size using precursor composition as the controllable parameter. In this context, the simulation approach demonstrated here may become a valuable tool for design of application-specific MoS_2 synthesis. Future studies may apply and extend the simulation technique to explore a wider range of conditions and materials, such as temperatures, substrates or other precursors. Finally, although this study focused on MoS_2 formation through thermal decomposition, the developed method can be extended to model other growth methods as well as other transition metal dichalcogenides (TMD). Such studies can fully characterize the effect of synthesis conditions on TMD domain size and enable understanding of the fundamental thermodynamic and kinetic mechanisms by which these conditions affect domain size.

Supporting Information: TEM post-processing details; drag calculation; effective Mo:S ratio calculation.

Acknowledgements: We acknowledge ExxonMobil Research and Engineering Company for fi-

nancial support of this work.

References

(1) Li, Y.; Wang, H.; Xie, L.; Liang, Y.; Hong, G.; Dai, H. MoS_2 nanoparticles grown on graphene: An advanced catalyst for the hydrogen evolution reaction. *J. Am. Chem. Soc.* **2011**, *133*, 7296–7299.

(2) Karunadasa, H. I.; Montalvo, E.; Sun, Y.; Majda, M.; Long, J. R.; Chang, C. J. A molecular MoS_2 edge site mimic for catalytic hydrogen Generation. *Science* **2012**, *335*, 698–702.

(3) Li, Y.; Li, Y.-L.; Araujo, C. M.; Luo, W.; Ahuja, R. Single-layer MoS_2 as an efficient photocatalyst. *Catal. Sci. Technol.* **2013**, *3*, 2214.

(4) Mak, K. F.; Lee, C.; Hone, J.; Shan, J.; Heinz, T. F. Atomically thin MoS_2: A new direct-gap semiconductor. *Phys. Rev. Lett.* **2010**, *105*, 136805.

(5) Radisavljevic, B.; Radenovic, A.; Brivio, J.; Giacometti, V.; Kis, A. Single-layer MoS_2 transistors. *Nat. Nanotechnol.* **2011**, *6*, 147–150.

(6) Zeng, H.; Dai, J.; Yao, W.; Xiao, D.; Cui, X. Valley polarization in MoS_2 monolayers by optical pumping. *Nat. Nanotechnol.* **2012**, *7*, 490–493.

(7) Yin, Z.; Li, H.; Li, H.; Jiang, L.; Shi, Y.; Sun, Y.; Lu, G.; Zhang, Q.; Chen, X.; Zhang, H. Single-layer MoS_2 phototransistors. *ACS Nano* **2012**, *6*, 74–80.

(8) Vazirisereshk, M. R.; Martini, A.; Strubbe, D. A.; Baykara, M. Z. Solid lubrication with MoS_2: A review. *Lubricants* **2019**, *7*, 57.

(9) Lauritsen, J. V.; Kibsgaard, J.; Helveg, S.; Topsøe, H.; Clausen, B. S.; Lægsgaard, E.; Besenbacher, F. Size-dependent structure of MoS_2 nanocrystals. *Nat. Nanotechnol.* **2007**, *2*, 53–58.

(10) Bhattacharya, D.; Mukherjee, S.; Mitra, R. K.; Ray, S. K. Size-dependent optical properties of MoS_2 nanoparticles and their photo-catalytic applications. *Nanotechnology* **2020**, *31*, 145701.

(11) Jaramillo, T. F.; Jorgensen, K. P.; Bonde, J.; Nielsen, J. H.; Horch, S.; Chorkendorff, I. Identification of active edge sites for electrochemical H_2 evolution from MoS_2 nanocatalysts. *Science* **2007**, *317*, 100–102.

(12) Khare, H. S.; Burris, D. L. The effects of environmental water and oxygen on the temperature-dependent friction of sputtered molybdenum disulfide. *Tribol. Lett.* **2013**, *52*, 485–493.

(13) Curry, J. F.; Argibay, N.; Babuska, T.; Nation, B.; Martini, A.; Strandwitz, N. C.; Dugger, M. T.; Krick, B. A. Highly oriented Mo_2 coatings: Tribology and environmental stability. *Tribol. Lett.* **2016**, *64*, 11.

(14) Lee, Y.-H.; Zhang, X.-Q.; Zhang, W.; Chang, M.-T.; Lin, C.-T.; Chang, K.-D.; Yu, Y.-C.; Wang, J. T.-W.; Chang, C.-S.; Li, L.-J.; et al., Synthesis of large-area MoS_2 atomic layers with chemical vapor deposition. *Adv. Mater.* **2012**, *24*, 2320–2325.

(15) Wang, X.; Feng, H.; Wu, Y.; Jiao, L. Controlled synthesis of highly crystalline MoS_2 flakes by chemical vapor deposition. *J. Am. Chem. Soc.* **2013**, *135*, 5304–5307.

(16) Zhan, Y.; Liu, Z.; Najmaei, S.; Ajayan, P. M.; Lou, J. Large-area vapor-phase growth and characterization of MoS_2 atomic layers on a SiO_2 substrate. *Small* **2012**, *8*, 966–971.

(17) Jeon, J.; Jang, S. K.; Jeon, S. M.; Yoo, G.; Jang, Y. H.; Park, J.-H.; Lee, S. Layer-controlled CVD growth of large-area two-dimensional MoS_2 films. *Nanoscale* **2015**, *7*, 1688–1695.

(18) Sun, J.; Li, X.; Guo, W.; Zhao, M.; Fan, X.; Dong, Y.; Xu, C.; Deng, J.; Fu, Y. Synthesis methods of two-dimensional MoS_2: A brief review. *Crystals* **2017**, *7*, 198.

(19) Li, X.; Zhu, H. Two-dimensional MoS_2: Properties, preparation, and applications. *J. Materiomics* **2015**, *1*, 33–44.

(20) Bezverkhy, I.; Afanasiev, P.; Lacroix, M. Aqueous preparation of highly dispersed molybdenum sulfide. *Inorg. Chem.* **2000**, *39*, 5416–5417.

(21) Ling, X.; Lee, Y.-H.; Lin, Y.; Fang, W.; Yu, L.; Dresselhaus, M. S.; Kong, J. Role of the seeding promoter in MoS_2 growth by chemical vapor deposition. *Nano Lett.* **2014**, *14*, 464–472.

(22) Najmaei, S.; Liu, Z.; Zhou, W.; Zou, X.; Shi, G.; Lei, S.; Yakobson, B. I.; Idrobo, J.-C.; Ajayan, P. M.; Lou, J. Vapour phase growth and grain boundary structure of molybdenum disulphide atomic layers. *Nat. Mater.* **2013**, *12*, 754–759.

(23) van der Zande, A. M.; Huang, P. Y.; Chenet, D. A.; Berkelbach, T. C.; You, Y.; Lee, G.-H.; Heinz, T. F.; Reichman, D. R.; Muller, D. A.; Hone, J. C. Grains and grain boundaries in highly crystalline monolayer molybdenum disulphide. *Nat. Mater.* **2013**, *12*, 554–561.

(24) Ji, Q.; Zhang, Y.; Gao, T.; Zhang, Y.; Ma, D.; Liu, M.; Chen, Y.; Qiao, X.; Tan, P.-H.; Kan, M.; et al., Epitaxial monolayer MoS_2 on mica with novel photoluminescence. *Nano Lett.* **2013**, *13*, 3870–3877.

(25) Lin, Y.-C.; Lu, N.; Perea-Lopez, N.; Li, J.; Lin, Z.; Peng, X.; Lee, C. H.; Sun, C.; Calderin, L.; Browning, P. N.; et al., Direct synthesis of van der Waals solids. *ACS Nano* **2014**, *8*, 3715–3723.

(26) Bollinger, M. V.; Lauritsen, J. V.; Jacobsen, K. W.; Nørskov, J. K.; Helveg, S.; Besenbacher, F. One-dimensional metallic edge states in MoS_2. *Phys. Rev. Lett.* **2001**, *87*, 196803.

(27) Liu, K.-K.; Zhang, W.; Lee, Y.-H.; Lin, Y.-C.; Chang, M.-T.; Su, C.-Y.; Chang, C.-S.; Li, H.; Shi, Y.; Zhang, H.; et al., Growth of large-area and highly crystalline MoS_2 thin layers on insulating substrates. *Nano Lett.* **2012**, *12*, 1538–1544.

(28) Zong, X.; Na, Y.; Wen, F.; Ma, G.; Yang, J.; Wang, D.; Ma, Y.; Wang, M.; Sun, L.; Li, C. Visi-

ble light driven H_2 production in molecular systems employing colloidal MoS_2 nanoparticles as catalyst. *Chem. Comm.* **2009**, 4536.

(29) Shi, Y.; Zhou, W.; Lu, A.-Y.; Fang, W.; Lee, Y.-H.; Hsu, A. L.; Kim, S. M.; Kim, K. K.; Yang, H. Y.; Li, L.-J.; et al., van der Waals epitaxy of MoS_2 layers using graphene as growth templates. *Nano Lett.* **2012**, *12*, 2784–2791.

(30) Khaemba, D. N.; Neville, A.; Morina, A. New insights on the decomposition mechanism of molybdenum dialkyldiThioCarbamate (MoDTC): A Raman spectroscopic study. *RSC Adv.* **2016**, *6*, 38637.

(31) Zhou, D.; Shu, H.; Hu, C.; Jiang, L.; Liang, P.; Chen, X. Unveiling the growth mechanism of MoS_2 with chemical vapor deposition: From two-dimensional planar nucleation to self-seeding Nucleation. *Cryst. Growth Des.* **2018**, *18*, 1012–1019.

(32) Wang, S.; Rong, Y.; Fan, Y.; Pacios, M.; Bhaskaran, H.; He, K.; Warner, J. H. Shape evolution of monolayer MoS_2 crystals grown by chemical vapor deposition. *Chem. Mater.* **2014**, *26*, 6371–6379.

(33) Govind Rajan, A.; Warner, J. H.; Blankschtein, D.; Strano, M. S. Generalized mechanistic model for the chemical vapor deposition of 2D transition metal dichalcogenide monolayers. *ACS Nano* **2016**, *10*, 4330–4344.

(34) Özden, A.; Ay, F.; Sevik, C.; Perkgöz, N. K. CVD growth of monolayer MoS_2: Role of growth zone configuration and precursors ratio. *JPN J. Appl. Phys.* **2017**, *56*, 06GG05.

(35) Zhu, D.; Shu, H.; Jiang, F.; Lv, D.; Asokan, V.; Omar, O.; Yuan, J.; Zhang, Z.; Jin, C. Capture the growth kinetics of CVD growth of two-dimensional MoS_2. *NPJ 2D Mater. Appl.* **2017**, *1*, 8.

(36) Michels, A.; Krill, C.; Ehrhardt, H.; Birringer, R.; Wu, D. Modelling the influence of grain-

size-dependent solute drag on the kinetics of grain growth in nanocrystalline materials. *Acta Mater.* **1999**, *47*, 2143–2152.

(37) Hillert, M. Solute drag in grain boundary migration and phase transformations. *Acta Mater.* **2004**, *52*, 5289–5293.

(38) Liu, F.; Kirchheim, R. Grain boundary saturation and grain growth. *Scr. Mater.* **2004**, *51*, 521–525.

(39) Dillon, S. An experimentally quantifiable solute drag factor. *Acta Mater.* **2008**, *56*, 1374–1379.

(40) Hansen, L. P.; Johnson, E.; Brorson, M.; Helveg, S. Growth mechanism for single- and multi-layer MoS_2 Nanocrystals. *J. Phys. Chem. C* **2014**, *118*, 22768–22773.

(41) Atkinson, H. Overview no. 65: Theories of normal grain growth in pure single phase systems. *Acta Metall.* **1988**, *36*, 469–491.

(42) Burke, J. E. Some factors affecting the rate of grain growth in metals. *Trans. AIME* **1949**, *180*, 73–91.

(43) Saber, M.; Koch, C. C.; Scattergood, R. O. Thermodynamic grain size stabilization models: An overview. *Mater. Res. Lett.* **2015**, *3*, 65–75.

(44) Kirchheim, R. Grain coarsening inhibited by solute segregation. *Acta Mater.* **2002**, *50*, 413–419.

(45) Liu, K.; Mücklich, F. Thermal stability of nano-RuAl produced by mechanical alloying. *Acta Mater.* **2001**, *49*, 395–403.

(46) Cain, J. D.; Shi, F.; Wu, J.; Dravid, V. P. Growth mechanism of transition metal dichalcogenide monolayers: The role of self-seeding fullerene nuclei. *ACS Nano* **2016**, *10*, 5440–5445.

(47) Li, X.; Zhang, S.; Chen, S.; Zhang, X.; Gao, J.; Zhang, Y.-W.; Zhao, J.; Shen, X.; Yu, R.; Yang, Y.; et al., Mo concentration controls the morphological transitions from dendritic to semicompact, and to compact growth of monolayer crystalline MoS_2 on various substrates. *ACS Appl. Mater. Inter.* **2019**, *11*, 42751–42759.

(48) Joo, P. H.; Cheng, J.; Yang, K. Size effects and odd-even effects in MoS_2 nanosheets: first-principles studies. *Phys. Chem. Chem. Phys.* **2017**, *19*, 29927–29933.

(49) Shirazi, M.; Kessels, W. M. M.; Bol, A. A. Strategies to facilitate the formation of free standing MoS_2 nanolayers on SiO_2 surface by atomic layer deposition: A DFT study. *APL Mater.* **2018**, *6*, 111107.

(50) Caturello, N. A. M. S.; Besse, R.; Da Silva, A. C. H.; Guedes-Sobrinho, D.; Lima, M. P.; Da Silva, J. L. F. Ab initio investigation of atomistic insights into the nanoflake formation of transition-metal dichalcogenides: The examples of MoS_2, $MoSe_2$, and $MoTe_2$. *J. Phys. Chem. C* **2018**, *122*, 27059–27069.

(51) Meuwly, M. Reactive molecular dynamics: From small molecules to proteins. *Wiley Interdiscip. Rev. Comput. Mol. Sci* **2019**, *9(1)*, e1386.

(52) Martini, A.; Eder, S. J.; Dörr, N. Tribochemistry: A review of reactive molecular dynamics simulations. *Lubricants* **2020**, *8*, 44.

(53) Ostadhossein, A.; Rahnamoun, A.; Wang, Y.; Zhao, P.; Zhang, S.; Crespi, V. H.; van Duin, A. C. T. ReaxFF reactive force-field study of molybdenum disulfide (MoS_2). *J. Phys. Chem. Lett.* **2017**, *8*, 631–640.

(54) Hong, S.; Krishnamoorthy, A.; Rajak, P.; Tiwari, S.; Misawa, M.; Shimojo, F.; Kalia, R. K.; Nakano, A.; Vashishta, P. Computational synthesis of MoS_2 layers by reactive molecular dynamics simulations: Initial sulfidation of MoO_3 surfaces. *Nano Lett.* **2017**, *17*, 4866–4872.

(55) Chen, R.; Jusufi, A.; Schilowitz, A.; Martini, A. Formation of MoS_2 from elemental Mo and S using reactive molecular dynamics simulations. *J. Vac. Sci. Technol. A.* **2020**, *38*, 022201.

(56) Plimpton, S. Fast parallel algorithms for short-range molecular dynamics. *J. Comput. Phys* **1995**, *117*, 1–19.

(57) Stukowski, A. Visualization and analysis of atomistic simulation data with OVITO-the Open Visualization Tool. *Model. Simul. Mater. Sci. Eng* **2010**, *18*, 015012.

(58) Nicolini, P.; Capozza, R.; Restuccia, P.; Polcar, T. Structural ordering of molybdenum disulfide studied via reactive molecular dynamics simulations. *ACS Appl. Mater. Inter.* **2018**, *10*, 8937–8946.

(59) Chen, W.; Zhao, J.; Zhang, J.; Gu, L.; Yang, Z.; Li, X.; Yu, H.; Zhu, X.; Yang, R.; Shi, D.; et al., Oxygen-assisted chemical vapor deposition growth of large single-crystal and high-quality monolayer MoS_2. *J. Am. Chem. Soc.* **2015**, *137*, 15632–15635.

(60) Xia, Y.; Xia, X.; Peng, H.-C. Shape-controlled synthesis of colloidal metal nanocrystals: Thermodynamic versus kinetic products. *J. Am. Chem. Soc.* **2015**, *137*, 7947–7966.

(61) Dang, K. Q.; Spearot, D. E. Effect of point and grain boundary defects on the mechanical behavior of monolayer MoS_2 under tension via atomistic simulations. *J. Appl. Phys.* **2014**, *116*, 013508.

(62) Cao, D.; Shen, T.; Liang, P.; Chen, X.; Shu, H. Role of chemical potential in flake shape and edge properties of monolayer MoS_2. *J. Phys. Chem. C* **2015**, *119*, 4294–4301.

(63) Tsafack, T.; Bartolucci, S. F.; Maurer, J. A. The role of molybdenum oxysulfide rings in the formation of two-dimensional molybdenum disulfide by powder vaporization. *J. Phys. Chem. A* **2018**, *122*, 7320–7327.

Graphical TOC Entry